

Interaction between nulls and emission in the pulsar B0834+06

Joanna M. Rankin^{1,2*} and Geoffrey A. E. Wright^{1,3*}

¹*Astronomical Institute ‘Anton Pannekoek’, University of Amsterdam, Kruislaan 403, 1098 SJ, Amsterdam, the Netherlands*

²*Physics Department, University of Vermont, Burlington VT 05405*

³*Astronomy Centre, University of Sussex, Falmer BN1 9QJ*

Accepted 2007 May 9. Received 2007 May 9; in original form 2006 December 22

ABSTRACT

We present a detailed study of the single pulses of the bright radio pulsar B0834+06, and offer evidence that the dominant periodic modulation in this pulsar’s emission governs the occurrence of nulls. The nulls of B0834+06 constitute approximately 9 per cent of the total pulses and we demonstrate that they do not occur at random in the pulse sequence. On the contrary, they are found to occur preferentially close to the minimum of the pulsar’s emission cycle, whose period jitters around a central value of $P_3 \approx 2.17$ rotation periods. It is likely that the intrinsic duration of the nulls averages about 0.2 times the pulsar rotation period. Surprisingly, the clearly distinct population of nulls and partial nulls of B0834+06 exhibit a two-peak profile slightly broader than that of the normal emission. This is in contrast to the profile of extremely weak normal pulses, which is narrower than the overall profile. A flow/counterflow model for the pulsar’s two components can reproduce the essential observed features of the emission in its dominant mode, with nulls occurring at the point where the minima of the two systems are aligned. This suggests that the observed nulling rate is determined by the chance positioning of our sightline with respect to the system. If the flow is interpreted as part of a circulating carousel, a fit yields a best estimate of 14 ‘sparks’.

Key words: MHD – plasmas – polarization – radiation mechanisms: non-thermal – methods: data analysis – pulsars: individual: B0834+06.

1 INTRODUCTION

The bright pulsar PSR B0834+06 was one of the first four pulsars to be discovered (Pilkington et al. 1968) and has therefore been a subject of study over many years. Its rotation period (P_1) of 1.27 s is relatively long, but its inferred physical properties (spin-down age τ , 3 Myr, surface magnetic field B_s , 3×10^{12} G) are close to average. Its profile, towards which it rapidly converges after only a few pulses, has two distinct peaks and appears typical of many pulsars. Yet an unusual feature is that the separation of its peaks remains virtually constant (at some 5°) from below 50 to 5000 MHz – in stark contrast to the more usual behaviour, where profiles narrow as the frequency rises (Mitra & Rankin 2002; hereafter MR02). However, here our intention is to focus on the star’s single pulse, or pulse-sequence (hereafter PS) behaviour rather than its integrated properties.

For some time it has been known that B0834+06 exhibits numerous individual ‘nulls’ – pulses with apparently zero emission and easy to identify by eye in this bright pulsar (e.g. Fig. 3 below). We estimate that nearly 9 per cent of the pulses of B0834+06 are

nulls.¹ In the general pulsar population the null proportion varies widely: in some up to 70–80 per cent of the pulses are nulls, yet in others nulls are completely absent (e.g. Rankin 1986; Biggs 1992; Redman & Rankin, in preparation). However, there is little, if any, correlation between the null fraction of a pulsar and that pulsar’s basic properties or geometry. Only the tendency of the null fraction to increase with spin-down age gives any statistical clue to their nature. It is perhaps unsurprising that the underlying physical agency responsible for nulls has remained a complete mystery.

However, clues to the provenance of nulls can be gleaned from studies of individual pulsars. One such is the observation that nulls, although unpredictable on a pulse-to-pulse basis, do not appear at random. In some pulsars, such as B0809+74, they tend to appear in successive pulses in sequences of varying length (Lyne & Ashworth 1983; van Leeuwen et al. 2002), while in others, such as B0818–13, they have a flickering on–off quality (Janssen & van Leeuwen 2004). Yet again, for example in B2303+30 (Redman, Wright & Rankin 2005, hereafter RWR), nulls are found to be correlated with the appearance of a more disordered emission mode. Furthermore, it has been shown that nulls subtly influence the emission which they

¹ This value is slightly larger than the 7.1 per cent given by Ritchings (1976) almost certainly owing to the improved quality of our observations.

*E-mail: joanna.rankin@uvm.edu (JMR); g.wright@sussex.ac.uk (GAEW)

interrupt, most especially in the pulses directly following the null (van Leeuwen et al. 2002, 2003), suggesting that nulls are produced within the system which generates the emission, and are not superimposed by some independent mechanism.

We therefore set out to investigate both the null statistics and the emission system of B0834+06, and to identify their interactions. Long ago this pulsar was found to undergo rapid emission fluctuations (hereafter P_3) of about two rotation periods in both its profile components (Taylor, Jura & Huguenin 1969; Slee & Mulhall 1970; Backer 1973). This ‘on-off’ property is shared by a number of pulsars, including B0943+10 and B2303+30, which have been studied in detail (Deshpande & Rankin 1999, 2001, hereafter DR99, DR01; RWR). However, the only recent detailed study of B0834+06 is that of Asgekar & Deshpande (2005; hereafter AD05), who were able to examine its single-pulse properties for the first time at the exceptionally low frequency of 35 MHz. Despite the observational difficulties, these authors were able to detect sufficient single-pulse sequences (comprising about 400 pulses in all) to confirm the regular emission modulation and to suggest a circulation time for a presumed underlying ‘carousel’ of subbeams.

At our observing frequency of 327 MHz the pulsar is naturally far brighter and nulls are easy to identify, even by eye. We therefore sought to verify the low-frequency results of AD05, and to explore what link, if any, exists between the emission cycle and the occurrences of nulls. In the next section we summarize our observations, followed by a detailed analysis of our results in Section 3, and discuss the conclusions and suggested interpretations in Section 4. Finally, we summarize our principal results in Section 5. Appendix A further discusses the pulsar’s emission geometry (Section A1) and the implications of the results in terms of a possible carousel-beam model (Section A2).

2 OBSERVATIONS

The observations used in our analyses were made using the 305-m Arecibo Telescope in Puerto Rico. The primary 327-MHz polarized PSs were acquired using the upgraded instrument together with the Wideband Arecibo Pulsar Processor² on 2003 October 5 and 2006 May 6, comprising 3789 and 1920 pulses, respectively. The auto- and cross-correlations of the channel voltages produced by receivers connected to orthogonal linearly polarized feeds were nine-level (three-level on May 6) sampled. Upon Fourier transforming, 128 channels were synthesized across a 25-MHz bandpass with a 1024- μ s (1.244-ms on May 6) sampling time, providing a resolution around 1 milliperiod of longitude. The Stokes parameters have been corrected for dispersion, interstellar Faraday rotation, and various instrumental polarization effects.

3 ANALYSIS

3.1 Basic properties

The familiar profile of B0834+06 over 3789 pulses is shown in Fig. 1. Its conal double (D) character is well known (Rankin 1983), and this together with the near constancy of its peak separation at all frequencies is indicative of an inner cone (MR02). Gradually, towards higher frequencies, the second peak gains in comparative strength, the interpeak bridge emission diminishes and the two peaks

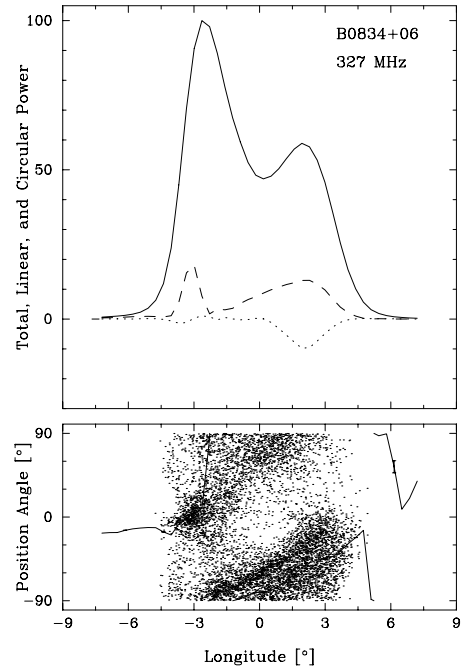


Figure 1. Integrated profile of 3789 pulses from B0834+06 at 327 MHz. The top panel gives the total intensity (Stokes I ; solid curve), the total linear (Stokes L ; dashed) and the circular polarization (Stokes V ; dotted). The lower panel PA histogram corresponds to those samples having PA errors smaller than 0.5° with the average PA curve overplotted.

become distinct and separated, so the widths of the two components must narrow slightly. Some high-frequency profiles also suggest weak outer cone emission (see MR02, note 3). Discovered at 80 MHz, B0834+06 can be observed over a remarkably large frequency range, but the claimed decametre interpulse emission (Bruck & Ustimenko 1979) has not been confirmed (Phillips & Wolszczan 1989; Hankins & Rankin 2006).

The lower panel of Fig. 1 gives a polarization position-angle (hereafter PA) histogram as well as the average PA traverse. Note that tracks corresponding to the two orthogonal polarization modes (hereafter OPM) are prominent, and the small aggregate linear polarization reflects their comparable intensities. The average PA shows a 90° jump under the leading component and fails to follow either track in the trailing part of the profile, showing that the two modes are not fully orthogonal.³ Granted, it is difficult to estimate a reliable PA sweep rate for this star, and easy to see from Fig. 1 how misleading are those based on the average PA traverse – a matter we will come back to in discussing the star’s emission geometry in Section A1.

In Fig. 2, we show the longitude-resolved fluctuation–power (hereafter lrf) spectra of the long 327-MHz PS. The modulation feature at a frequency of 0.461 cycles/ P_1 , equivalent to a P_3 periodicity of $2.1695 \pm 0.0003 P_1$, is evident in both profile peaks – in general agreement with the results of AD05. We also computed a harmonic-resolved fluctuation spectrum (not shown), similar to AD05’s Fig. 2, and this shows a smaller peak at some 0.539 (or -0.461) cycles/ P_1 , suggesting as expected that the lrf feature represents a mixture of phase and amplitude modulation. Note that

³ A similar result was reached by Gil et al. (1992) though we now know that the old 430-MHz AO polarimetry was unreliable in this case – witness the ‘flat’ PA trajectory they discuss for B0834+06.

² <http://www.naic.edu/~wapp>

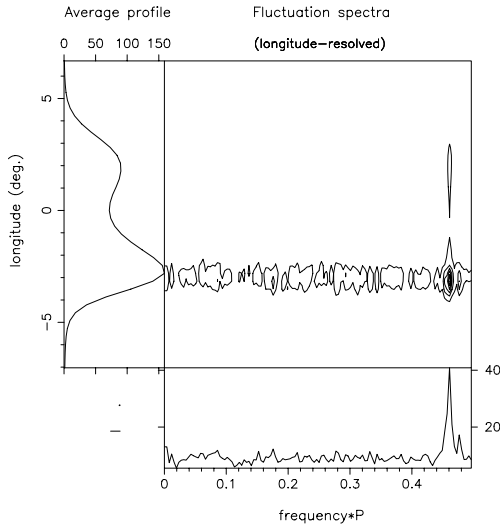


Figure 2. Longitude-resolved fluctuation spectra for B0834+06 at 327 MHz, computed using the same 2003 October 5, 3789-pulse observation as in Fig. 1. The analysis was applied to the total power (Stokes I) and used an FFT of length 256. The three panels give the pulsar’s average profile (left-hand side), lrf spectra (centre) and integral spectrum, (bottom), respectively. The central panel uses eight contour levels.

this modulation feature has a broad base (and even another weaker component), indicating the presence of nearby alternative or secondary periodicities present in the PS (see also Weltevrede et al. 2006, 2007). There is also a slight enhancement of power at fluctuation frequencies between 0.03 and 0.1 cycles/ P_1 . This may arise from aliasing of the principal frequency since its value is so close to $2P_1$ – but nothing as prominent as the $0.07P_1$ feature found by AD05 in one of their relatively short observations can be seen in Fig. 2.

3.2 Pulse sequences

Since the fluctuation spectrum of Fig. 2 taken over 3789 pulses is dominated by the $P_3 \approx 2$ feature, one might expect the detailed behaviour of B0834+06 to be a steady on–off emission in each component – much as in B0943+10, where the single pulses (in its B mode) are highly organized in an unrelenting on–off pattern at the fundamental P_3 close to $2P_1$ and never null.

B0834+06 is much more volatile. To illustrate this, in Fig. 3 we show two different 201-pulse sequences extracted from our long 327-MHz observation. The nulls appear as white lines, so are easy to detect by eye. It also appears that some of the nulls are partial – that is, there is zero emission in only one component, which both here and in other PSs is usually the second component. It can be seen that the sequences share similar features: both have irregular individual nulls and irregular emission patterns with no consistent subpulse ‘drift’ (in which a subpulse apparently retains its identity by making a slight shift in phase in successive pulses). Here and there, in both PSs, evidence of the two-period modulation can be seen, and, surprisingly, this is present in the null patterns too. The bunching of nulls into double and even triple alternations is reminiscent of that found (by Janssen & van Leeuwen 2004) in B0818–13, though here the null frequency is 9 per cent against 1.6 per cent in that pulsar.

However, the fluctuation–power spectra of the PSs in Fig. 3 are strikingly different (cf. Fig. 4). The first sequence (to the left-hand side) has no dominant periodicity in either component, whereas the

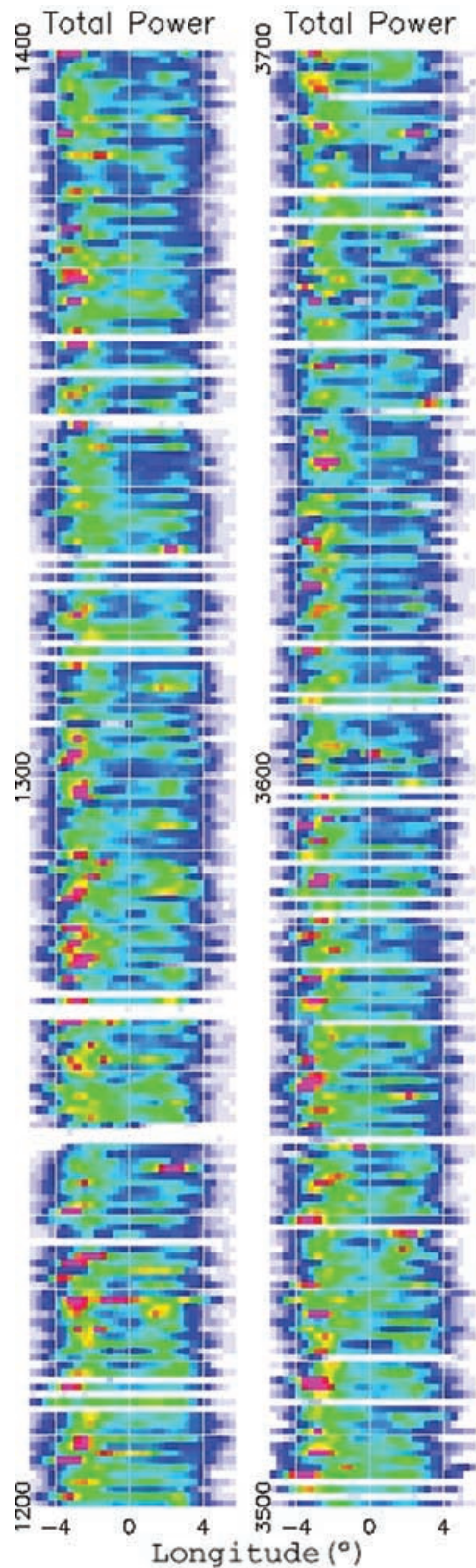


Figure 3. Total intensity displays of B0834+06 at 327 MHz on 2003 October 5: two different PSs of 201 pulses each are shown. Note the strange prevalence of nulls in alternate successive pulses – two groups of three in the left-hand PS – as well as the apparent partial nulls. The left-hand PS (pulse # 1200–1400) shows a strong even–odd modulation; whereas this is less clear in the right-hand sequence (# 3500–3700).

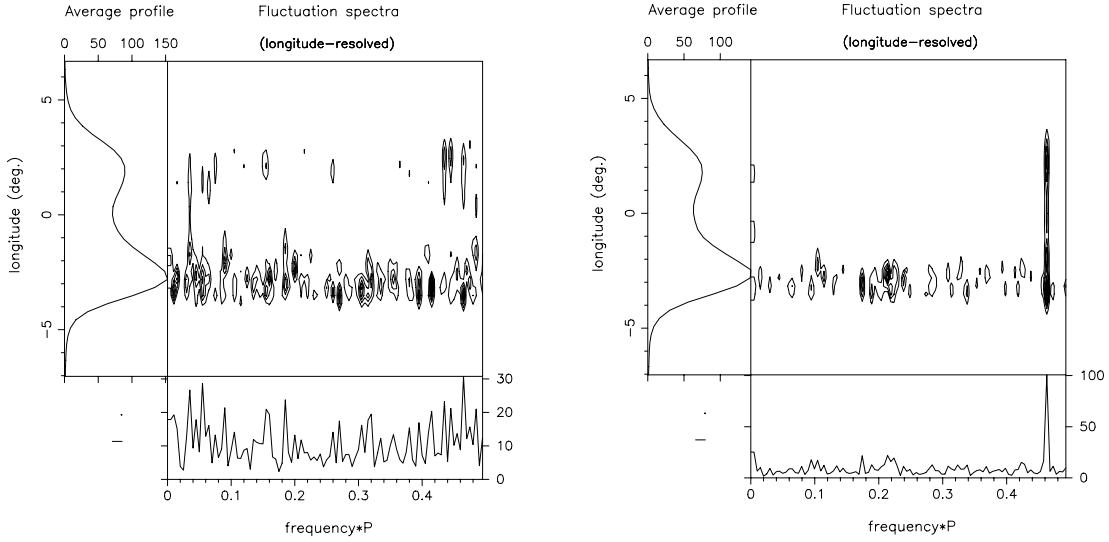


Figure 4. Lrf spectra for the two 201-pulse PSs in Fig. 3. Remarkably, the left-hand sequence (left-hand panel) for pulses 1200–1400 lacks a clear fluctuation periodicity, though a tendency for odd–even modulation is apparent; whereas that for pulses 3500–3700 in the right-hand PS (right-hand panel) exhibits strong regular fluctuation power in both components at the usual frequency of 0.461 cycles/ P_1 despite the weaker visual impression of alternate-pulse modulation in Fig. 3.

right-hand one exhibits the usual strong P_3 of $2.170 \pm 0.009P_1$ in both components, precisely the overall peak in Fig. 2. The point we wish to make is that although regular PSs similar to the right-hand one dominate our observations, there is an element of ‘jitter’ in the precise value of P_3 and occasionally P_3 is indeterminate, as in the left-hand sequence. On investigation, we discovered that such sequences still retain the underlying modulation at weak locations in the profile, but that at the component peaks a stronger, apparently random, intensity modulation is superimposed. This then creates a forest of peaks in the lrf spectra for 50–200 pulses. The overlaid intensity could not be radio frequency interference (RFI), since the entire signal was dispersed to the same degree. Furthermore, these changes are impossible to detect by eye.

We therefore examined carefully the changing fluctuation–power spectra throughout our observations, and there appeared to be four main emission behaviours. First, the primary behaviour having a P_3 of $2.170P_1$ is observed. Secondly and thirdly are intervals with P_3 values just over 2.207 and just under $2.098P_1$. These less frequent periodicities are then reflected in the broad lrf spectral peak of the entire PS in Fig. 2. Finally, the fourth behaviour is a ‘chaotic’ one such as that in the left-hand PS of Fig. 3, where multiple periodicities are present, probably occurring during intervals of transition. These behaviours should not be seen as ‘modes’ in the sense of the well-known and dramatic modes of B0329+54, B1237+25 or B2319+60, for example, when profile changes occur in association with fundamentally different subpulse modulation. They rather represent small fluctuations in the emission-cycle frequency close to $2P_1$, with short PSs of ‘chaos’ occurring when transitions are taking place: as the principal frequency fluctuates, the power spectrum will exhibit ‘forests’ of peaks until the main periodicity is regained.

Fluctuation spectra only tell part of the story: although the dominant $P_3 \approx 2$ in both Fig. 2 and the right-hand panel of Fig. 4 extend across both components, this gives us no information concerning the relative phase of the modulations in these components. However, this can be seen graphically by folding the right-hand PS in Fig. 3 at the peak P_3 of the right-hand panel of Fig. 4 (comprising about 100 fluctuation cycles). The result (Fig. 5) shows the inten-

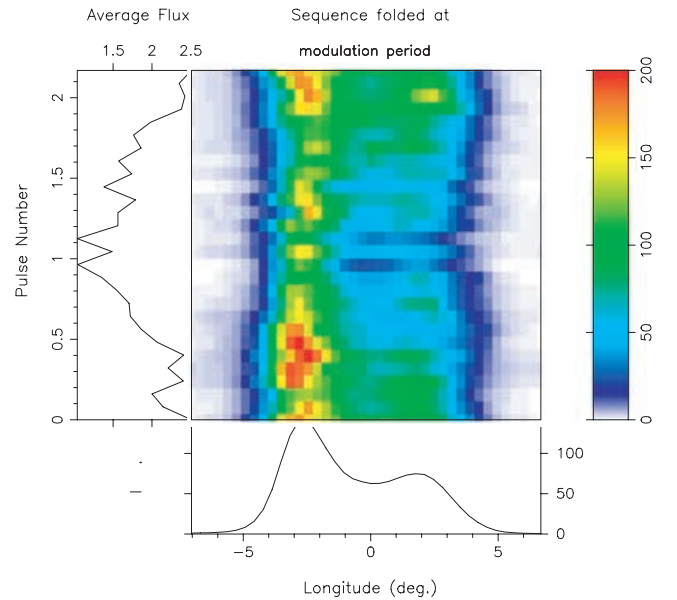


Figure 5. Fluctuation power as a function of longitude (centre) for the right-hand (# 3500–3700) PS of Fig. 3 over the $2.1695P_1$ modulation cycle. The average power (left-hand panel) fluctuates by about a factor of 2. The bottom panel shows the average profile. The emission in the trailing component lags that in the leading component by about half a period. Note also the presence of a ‘null zone’ between about 0.9 and 1.2 periods, suggesting that the intrinsic duration of a null is considerably less than half a rotation period.

sity peaks at differing phases of the cycle in each component, with the first component lagging the second by about $0.5P_1$. What is of particular interest is the deep emission minimum which occurs at the *same* phase in both components about $0.8P_1$ after the peak of the leading component. This results from the folding of the full and partial nulls, and convincingly demonstrates that the nulls participate in the $2.170P_1$ emission cycle. It also strongly suggests that the

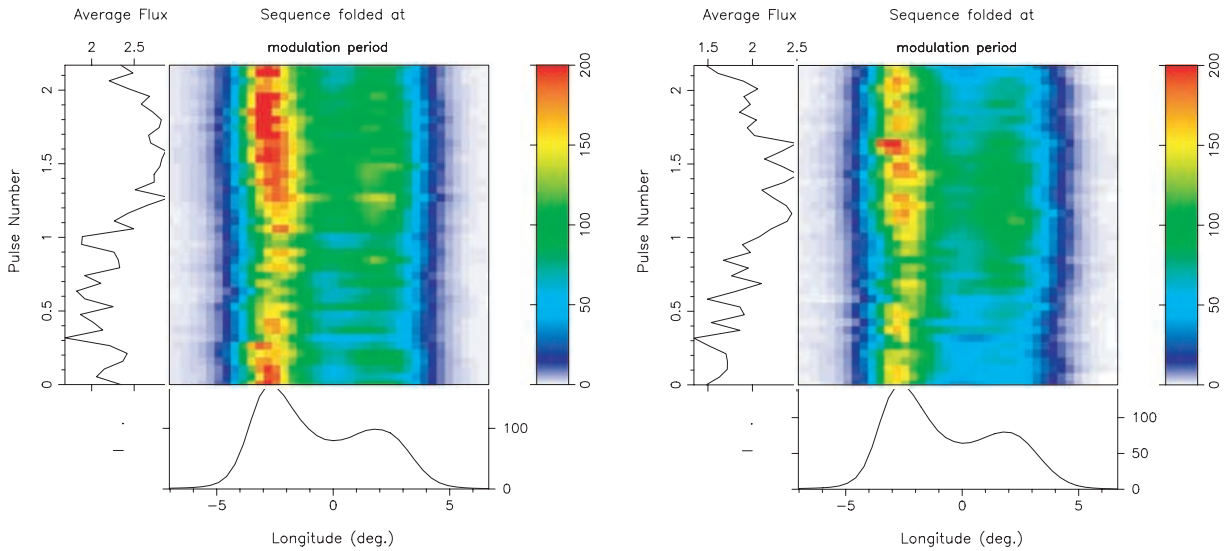


Figure 6. Fluctuation power as a function of longitude as in Fig. 5 for the two other long intervals with a P_3 of $2.170P_1$: left-hand panel, pulses 500–1400 and right-hand panel, pulses 3200–3789. Note the similar behaviour in these folded PSs to that in Fig. 5, especially the slight narrowing of the emission band towards the cycle minimum.

true duration of a null is substantially less than P_1 , possibly around $0.2P_1$. This is consistent with our observed null fraction of 9.3 per cent multiplied by the dominant cycle length of $2.17P_1$.

Folding our full 3789-pulse observation at the peak fluctuation period in Fig. 2 gives only a blurred pattern, since phase is lost many times as the fluctuation period ‘jitters’ and the ‘chaotic’ PSs, although brief, randomly adjust phase information. However, in our main 327-MHz observation there are two relatively long intervals in which the primary $2.170P_1$ modulation is stable – with lengths of some 900 and 600 periods, respectively, and separated by 2000 pulses (in total about 40 per cent of the PS) – and we folded each at P_3 . The results are shown in Fig. 6. The phases have been adjusted so that each has its minimum at the same point of the modulation cycle. As in the folded short sequence shown in Fig. 5, they have a peak delay of some $0.5P_1$ between the components, and the leading component peak precedes the cycle minimum by around $0.8P_1$. Given that they comprise 450 and 300 emission cycles, respectively, they are remarkably similar in form, both to each other and to Fig. 5, and indicate that the underlying pattern for the basic emission mode is clearly phase-shifted between the components and, yet again, that nulls are an integral property of the cycle. What we especially note, however, is that the nulls – by definition – are at the same phase of the cycle in each profile component, whereas the emission peaks have a clear phase shift.

3.3 Null distribution

Fig. 7 gives a null histogram for our long observation. 41 pulses have been excluded as a result of identifiable interference or bad baselines, so the remaining 3748 pulses are very well behaved in their statistical properties. Note that the noise distribution has a half-intensity width hardly 1 per cent of the average-pulse intensity. None the less, we see interestingly that the null distribution is skewed in the positive direction and indeed appears to continue at a low level to meet the pulse distribution. Some of these very low-intensity pulses are undoubtedly the partial nulls we encountered earlier, but the null distribution itself appears to retain some positive power.

With the statistics from the previous sections it is possible to test the hypothesis that the partial nulls may result from our sightline intersecting the pulsar’s beam just as a null is starting or ending. From the previous analysis we estimate the mean null length to be $0.2P_1$, or 72° of the duty cycle, and the emission beam is 10° wide. If in Fig. 7 we take the boundary between nulls/partial nulls and normal pulses to be the distribution’s minimum, which is located at the vertical $0.24\langle I \rangle$ dotted line, we include some 349 nulls or partial nulls with power falling below this threshold. Assuming a partial null must have at least half a pulse consisting of a null, their number will be of the order of $10^\circ/72^\circ \times 349$, or 48 pulses. This is consistent with the total of 40 partial nulls with intensities between 0.05 and $0.24\langle I \rangle$.

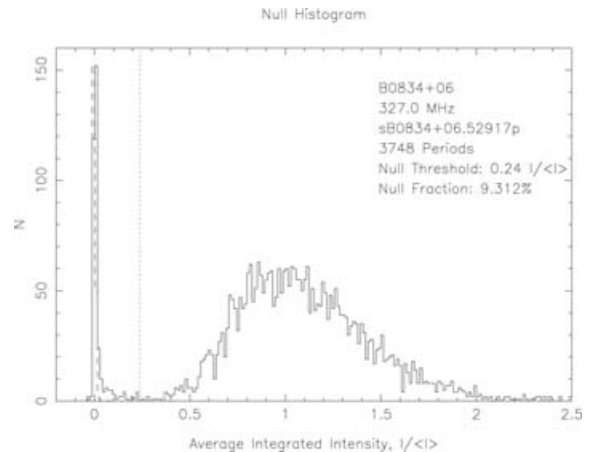


Figure 7. Traditional null histogram for the 3789-pulse observation (39 pulses were excluded from this histogram because of bad baselines or interference). The pulse-intensity distribution is shown by a solid line and that of the off-pulse noise distribution by a dashed line. Note the skewed shape of the null distribution and the largish ‘partial null’ population lying in between the respective tails of the pulse and null distributions. The vertical dotted line at an average-intensity level of $0.24\langle I \rangle$ represents the threshold below which pulses are taken as nulls or partial nulls for the purpose of constructing their average profile in Fig. 9.

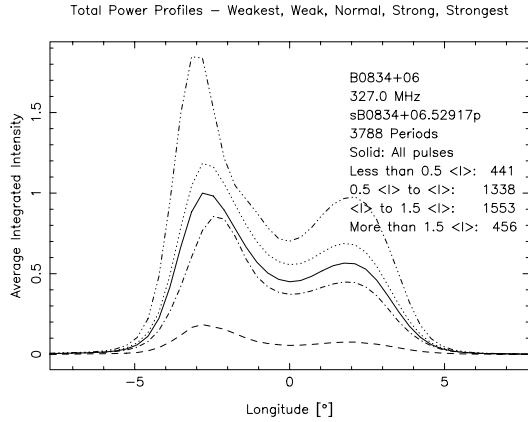


Figure 8. Average profiles comprising all pulses falling between the displayed intensity ranges. Note the gradual narrowing of the profile as the intensity range falls. The filled line is the mean profile.

The nulls and partial nulls occur close to the emission cycle minimum, as can be seen in Figs 5 and 6, and one might expect such pulses to share the characteristics of the weak emission which precede and follow them. In Fig. 8 we show integrated profiles obtained for different pulse-energy ranges. The profiles clearly become narrower as their energy range decreases. Hence partial nulls should have an even narrower profile, continuing the progression.

Surprisingly, the outturn is very different. The average profile of all pulses with intensity $<0.24 \langle I \rangle$ is plotted in Fig. 9. As might be expected, these pulses show a weak but very clear approximate signature of the star’s profile – not only in total power but also in linear polarization, a result which is found to be essentially unchanged even when the boundary is moved as close as $0.05 \langle I \rangle$. However, the pulses form a profile wider even than the maximum intensity profile of Fig. 8. This suggests that B0834+06’s nulls may differ from the nulls seen in other pulsars wherein no significant power can be detected in the average of many nulls.

3.4 Statistics of null-emission interaction

To further investigate the interaction between nulls and emission, we examined the statistical distribution of the nulls within our obser-

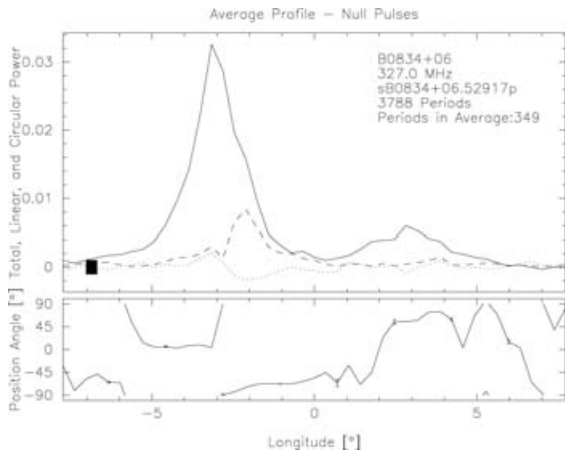


Figure 9. Average polarized profile comprising all null and partial null pulses falling below the intensity threshold in Fig. 7. The top panel shows the total intensity, linear power and circularly polarized power, and the bottom panel gives the polarization angle.

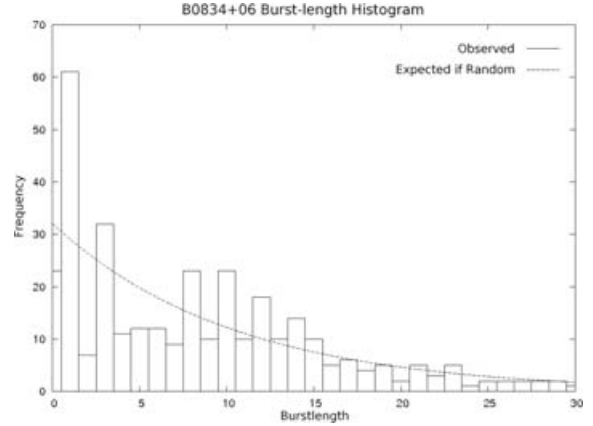


Figure 10. Histogram of the measured distribution of burst lengths among the 3789 pulses of our long 327-MHz observation. Superimposed (as a dotted line) is the expected frequency of burst lengths if the nulls were distributed randomly within the PS with a 9.2 per cent frequency.

ations in a manner similar to that used by (Janssen & van Leeuwen 2004) in their study of the characteristic null bunching in B0818–13. However, unlike their study (and because in B0834+06 we are dealing with a much higher rate of nulling), we did not focus exclusively on PSs where nulls were particularly dense but considered the statistics of the entire PS. We measured the lengths of ‘bursts’ of emission which occurred between one null (or partial null) and the next, and used the results to create a histogram of their relative frequency. The result is shown in Fig. 10, and for comparison we have superposed the expected frequency if the nulls were randomly distributed throughout the PS. The random distribution is a power law based on the assumption of a 9.2 per cent chance of each pulse being a null. Two successive nulls are most likely, then two nulls separated by a single pulse, etc. From Fig. 10 it is immediately clear that the nulls do not occur randomly. Most obviously, there is an excess of bursts with a duration of one pulse, and a shortfall of burst length zero (successive null pulses). However, there are also some unexpected peaks in the histogram for burst lengths 8, 10 and 12.

The explanation for these lies in the beat interaction between the pulsar rotation period P_1 , which is our natural sampling rate, and the underlying emission modulation period P_3 , which peaks at $2.17P_1$. If we crudely designate 9.2 per cent around the minimum of the cyclic emission pattern of Figs 5 and 6 to be the ‘null zone’, then once the observer samples a null in this region, she/he will probably next sample a null not in the next pulse, but after *two* pulses. This will occur not only for the principal $2.17P_1$ mode, but in any mode in which the underlying modulation has a P_3 close to $2P_1$. This is the reason for the large peak at burst length one, and again at three.

Later peaks depend more subtly on the precise P_3 . For the principal $2.17P_1$ modulation the best chances of sampling further nulls (assuming a null was missed after a burst length of one or three) will occur when the emission has passed through 5, 6 or 7 cycles – that is, after 10.85, 13.01 or 15.18 rotation periods – resulting in the observed burst lengths of 10, 12 or 14. After three cycles the null would occur at 6.5 periods, and thus would probably miss at burst lengths 5 or 6. For the second modulation mode with a P_3 of $2.2069P_1$, nulls will most likely reappear after 4, 5 or 6 cycles, that is, 8.83, 11.03 or 13.24 periods, giving peaks at burst lengths 8, 10 and 12. In general, the closer P_3 is to $2P_1$, the further the secondary peaks in the distribution will shift to larger burst length

values. Moreover, any P_3 close to $2P_1$ will generate peaks at even burst lengths, P_3 close to $3P_1$ will give peaks at multiples of 3, etc.

Thus the histogram of Fig. 8 represents a succinct and independent method for demonstrating the cyclic nature of the nulls of B0834+06. However, the presence of many burst lengths which do not conform to a simplified model above must be taken into account. The most obvious contradiction to the simple model is the significant number of bursts of zero length, that is, contiguous nulls. On inspection of the PSs we found that these never occurred when the pulsar was in its ‘principal mode’. Hence, we must assume that they only occur as the result of some disruption to the cyclic pattern (as in the left-hand sequence of Fig. 3).

Finally, our analysis easily affords the possibility of producing an artificial PS wherein the null pulses (with power falling below a predetermined noise threshold) are filled with the last non-null pulse. We recomputed the fluctuation spectra given above as well as a number of others. Generally, the fluctuation frequency did not change; however, its amplitude diminished substantially. The null-filled spectra corresponding to Figs 2 and 4 (right-hand panel) (not shown) do not appear very different qualitatively, but the intensity scales on the bottom panels are in each case reduced by about a factor of 2. The P_3 feature persisted, albeit more weakly, even when the non-null pulses were filled with the scaled-down average profile (and the partial nulls with the leading or trailing part of it) as in Herfndal & Rankin (2007) and Herfndal & Rankin (in preparation). Again, these analyses are strong evidence first that the nulls participate in the star’s pulse-to-pulse fluctuations, and secondly that they are not solely responsible for producing them.

4 DISCUSSION

4.1 Modelling B0834+06’s nulls

In the preceding section we have demonstrated three basic points. First, that the principal fluctuation mode of the pulsar results from a repeated cycle of emission some $2.17P_1$ in duration, which we demonstrated by folding the data at this frequency in substantial pulse sequences where this feature was strong and uninterrupted (see Fig. 6, also Fig. 5). This revealed a phase shift of about $0.5P_1$ between the maxima of the leading and trailing profile components, and a zone in the cycle, some $0.8P_1$ before the trailing component maximum, in which nulls tend to fall. Secondly, that the null distribution is fundamentally bimodal (Fig. 7), and together the nulls and partial nulls have an essentially different average profile (Fig. 8) from those of the weakest pulses of the normal pulse distribution (Fig. 9). Thirdly, that the full ensemble of our data reveals highly non-random patterns of nulls and intervening emission bursts which could only be produced by nulls which are integrated into a $P_3 \approx 2P_1$ emission cycle (Fig. 10).

These results are somewhat paradoxical. On one hand, the evidence that the nulls and partial nulls participate in the $2.17P_1$ cycle is incontrovertible (from the first and third points above). On the other hand, they have characteristics very different from normal pulses: not only do they possess a wider profile than that of weak normal pulses, but also they do not – by their very nature – exhibit an emission phase shift between the two profile components (otherwise the PS would contain numerous half-nulls instead of nulls).

However, there is a way out which may reveal something about the nature of nulls. In emission maps such as Figs 5 and 6 it is tempting to suppose that they represent the physical passage of two parallel beams (for the leading and trailing components) with

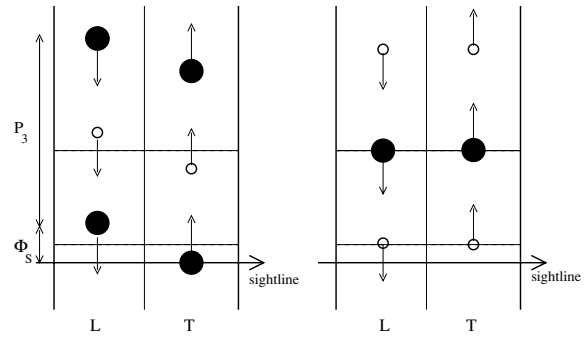


Figure 11. Schematic model of flow and counterflow across the observer’s sightline. The leading beam (L) and trailing beam (T) are assumed to have regularly spaced emission peaks, shown by dark circles, and minima by open circles. The two dotted lines indicate the two locations where the peaks/minima are instantaneously aligned during the P_3 cycle. The chance position of the observer’s sightline is determined by measuring Φ_s , the phase by which the peak of the trailing beam is observed to lead that of the leading beam (left-hand picture). At a time $(P_3 - \Phi_s)/2$ after the leading beam crosses the sightline, the minima will align on the lower dotted line just $\Phi_s/2$ from the observer’s sightline (right-hand picture). Using the observed values of P_3 and Φ_s , this instant is found to fall in the ‘null zone’ of Figs 5 and 6.

the arrow of time from bottom to top. However, this is only the observer’s perception. In reality it is possible that the leading beam is passing across the observer’s sightline from top to bottom and the trailing beam from bottom to top (or vice versa). We represent this in Fig. 11.

As the beams pass one another, there are *two* moments within the cycle period (P_3) when the two-beam systems are instantaneously aligned. These moments are fixed by the system, and are independent of the position of the observer’s sightline. The dotted lines indicate the two phases at which either both peaks or both minima alternately align.

The left-hand picture represents the instant when the maximum intensity point of the trailing beam crosses the sightline from below, just a phase Φ_s before the maximum of the leading beam crosses from above. *The magnitude of this phase delay is fixed by the chance positioning of our sightline with respect to the beam system, and not by any intrinsic features of the beam system itself.* The first alignment following this instant will bring the two peaks together on the lower dotted line (after phase $\Phi_s/2$), and, if sampled on our sightline, the observed intensity will be strong (since $\Phi_s \approx 0.5P_1 \ll P_3 \approx 2.17P_1$ for B0834+06).

The second alignment occurs a further $P_3/2$ later and is illustrated on the right-hand picture of Fig. 11. Now the emission minima of both beams are aligned at the position of the lower dotted line, close to the observer’s sightline. In fact, it is easy to show that the alignment of the minima must fall equidistant from the last peak in the leading component and the next peak in the trailing component by a phase distance of $(P_3 - \Phi_s)/2$ or $0.85P_1$ – a figure which places the alignment within the ‘null zone’ of all three images of the emission cycle in Figs 5 and 6.

This result implies that if we used the model of Fig. 11 to generate a *pseudo*-sequence of pulses, insisting on a null whenever the sightline sampled the emission close to an alignment of the minima, then we could mimic the stable pulse sequences of B0834+06, the resulting folds of Figs 5 and 6, and indeed the histogram peaks of Fig. 10. Note that partial nulls should now be seen as the result of the sightline passing close to a minimum in one of the components, but inevitably being somewhat further from the minimum of the other.

Our conjecture is therefore that nulls and partial nulls are observed in B0834+06 when our sightline samples emission close to an alignment of the minima of the two beams. This is made possible by the chance positioning of our sightline with respect to the beam system. If the system of B0834+06 were instead observed with $\Phi_s \approx 0.5P_3 \approx 1.08P_1$, we would see an alternating system with peaks appearing successively in the leading and trailing components – but nulls would not be observed. This is close to what is seen in the dominant (B) mode of B2303+30 (RWR). If, by contrast, $\Phi_s \approx 0$ then our sightline would sample nulls more frequently and flickering would be more common. This hints at why a pulsar's null rate so little correlates with its basic parameters.

A further interesting consequence of this model is that it expects the null fraction to depend slightly on the observing radio frequency (if a radius-to-frequency mapping is present). Assuming the beams lie on cones of open magnetic field lines, then, as the observing frequency changes, the widening of the field lines will cause our sightline's relative position to the cycle to shift. The sightline will shift closer to or further from the cycle minimum, depending on whether our sightline lies between the cone axis and the rotation axis or not. Frequency-dependent nulling has been reported in B0809+74, a prominent drifter (Davies et al. 1984), and recently in B1133+16 (Bhat et al. 2007), a double-peak pulsar very similar to B0834+06 in its basic parameters and with a null fraction of about 15 per cent.

In B0834+06 the cycle length (P_3) appears to jitter. In the model of Fig. 11 a speeding-up or slowing-down of the cycle will not alter the relative position of the sightline, since the cycle structure will expand or shrink in proportion to P_3 (assuming the flow and counterflow have the same P_3). This will only alter the observation of nulls if this depends on the absolute (rather than relative) difference of phase between the sightline's position and the minimum alignment, and we have no way of knowing whether this may be so. What would change the number of nulls observed is an instability such that the P_3 of the flow and counterflow were temporarily different, since this would shift the phase at which the minima aligned. In B2303+30, the B mode with $P_3 \approx 2P_1$ frequently shifts to a Q mode with $P_3 \approx 3P_1$ (RWR). The stable sequences of the second mode show few nulls, as in the principal mode, but the rapid oscillating transitions which accompany the switch exhibit frequent nulls.

In fact, many pulsars have P_3 values which are 'quantized' and their emission rapidly switches from one pattern to another. Such switches could alter the observed null rate only if the change in mode was accompanied by a shift in the field lines on which the various modes appeared, affecting both the absolute and relative position of our sightline with respect to the locus of the minima. This has been claimed in at least one pulsar (B0809+74), in which transitions are often accompanied by nulls. But the application of the present model to nulls in this and other single-peaked pulsars is beyond the scope of this paper.

Although we now have a logically consistent model for the observed steady patterns of emission and nulls in B0834+06, we must still consider why nulls and partial nulls integrate to a wider profile than that found at the minimum of the emission cycle. Of course, we need not assume that nulls are *inevitably* triggered when the alignment occurs: it could be that they are linked to a further geometric condition, requiring a greater separation between flow and counterflow. Alternatively, the symmetric alignment may briefly change the underlying physical system (even momentarily slowing or halting the cycle). In the classic model of Ruderman & Sutherland (1975), the drifting regions (i.e. the flow and counterflow) are driven by a motion which relies on a differential electric field perpendicular to the magnetic field lines. Possibly, when the so-called 'sparks'

achieve symmetry about the rotation axis, this potential temporarily weakens and the drift ceases.

4.2 The carousel model

It is important to note that the structure of the model in Fig. 11 does not automatically imply the presence of an underlying circulating carousel of sparks in B0834+06. We observe no drift of the emission between the components of the pulsar (see Fig. 3), and we could not convincingly demonstrate any consistent delay in correlations between their intensities. Hence the time-reversed systems represented in Fig. 11 may somehow exist independent of each other. However, the geometry of pulsar polar regions naturally suggests that they are connected.

The model of Wright (2003), for example, would connect the two beams without requiring them to drift: a near-stationary carousel is possible, the result of a steady auroral feedback system between inner and outer regions of the magnetosphere. Here, emission modulations would result not from drift of beamlets, but from regular patterns in the flow which streams to and from the inner and outer 'nodes' of the system (see Fig. 4 of Wright 2003). Nulls would arise in one or other of the components if there were gaps in the flow, temporarily interrupting the pair creation which is the engine of the model.

However, by far the longest established model (Ruderman & Sutherland 1975) for pulsar modulations is the circulating carousel of 'sparks', and we attempted to see if a geometry based on it could be fitted to our observations, not least because it has successfully been applied (DR99, DR01) to the highly regular modulations of PSR B0943+10. Ideally, such a fit requires the presence of a clear low-frequency feature in the fluctuation spectra, which could then be interpreted as indicating a carousel circulation time, and makes the assumption that intensities of the individual sparks are maintained over time periods at least of the order of the circulation time. Neither of these points could be relied upon here: B0834+06 resembles B0943+10 in that it has a P_3 close to $2P_1$, but this value was not stable over the observation duration, and its lrf feature is not as narrow as that of B0943+10, so indications of a long-period cycle were far harder to identify.

The results we obtained for B0834+06 are given in Section A2. By matching the model to the observations in sequences with clear P_3 values we identified a best fit for the circulation time of $30.3P_1$. This would suggest that 14 'sparks' or beamlets are circulating around the magnetic pole. In Appendix A, one can see the folds and carousel patterns that this result implies. Despite considerable efforts, we can only say we have optimized the likely value for the true circulation time. The occasions of 15 or $30P_1$ modulations which led us to our result are neither frequent nor persistent, nor strong when they appear. A weak $30-P_1$ lrf feature is seen in the longer PS when the non-null pulses are filled with the average profile (Herfindal & Rankin, in preparation). Quite possibly, the inherent volatility in the emission of the beamlets prevented a clearer result.

5 SUMMARY OF RESULTS

Our principal results can be summarized as follows.

(1) Approximately 9 per cent of the pulses of B0834+06 can be classified as nulls (see Figs 3 and 7). A small fraction of these nulls are 'partial' in the sense of still having faint emission, usually in only one of the profile components, yet not belonging to the tail of the distribution of normal pulses.

(2) The emission of the pulsar is modulated over a period of $P_3 \approx 2.17P_1$, present in both its components with a phase difference of roughly $0.5P_1$ between them (see Figs 2, 5 and 6).

(3) The nulls participate in the P_3 modulation cycle: they preferentially occur when the emission is close to the minimum of its cycle and probably have a true duration averaging around $0.2P_1$ (see Fig. 5). The closeness of P_3 to $2P_1$ means that they often appear in alternating pulses.

(4) The nulls are not randomly distributed through the pulse sequence, there being too many alternating nulls and not enough contiguous nulls for a random expectation (see Fig. 10).

(5) Profiles formed from weak normal pulses are narrower than those formed from strong pulses (see Fig. 8). However, nulls and partial nulls form a profile wider than even the strong pulses (see Fig. 9). Thus partial nulls, though possessing weak emission, are not simply extremely weak normal pulses.

(6) We demonstrate that the steady behaviour of B0834+06 can be successfully reproduced by modelling its two components as two identical emission cycles, one of which is the time-reverse of the other (Fig. 11). These are aligned twice within the P_3 cycle. Nulls occur when our sightline samples at a phase close to the alignment of the two minima.

(7) If the emission cycle is seen as a rotating carousel of ‘beamlets’ about the magnetic pole, the most likely circulation time (\hat{P}_3) is about $30P_1$. Though not clearly established, this implies the presence of 14 ‘beamlets’ (see Fig. A2).

ACKNOWLEDGMENTS

We thank Ben Stappers and Patrick Weltevrede for interesting and useful discussions, and Avinash Deshpande, Jeffrey Herfindal and Stephen Redman for assistance. GAEW is grateful to the Astronomy Centre, University of Sussex, for a Visiting Fellowship. Much of the work was made possible by visitor-grant support from the Netherlands Organisatie voor Wetenschappelijk Onderzoek and US National Science Foundation Grants AST 99-87654 and 00-98685. Arecibo Observatory is operated by Cornell University under contract to the US NSF. This work made use of the NASA ADS astronomical data system.

REFERENCES

- Asgekar A., Deshpande A. A., 2005, MNRAS, 357, 1105 (AD05)
 Backer D. C., 1973, ApJ, 182, 245
 Bhat N. D. R., Gupta Y., Kramer M., Karastergiou A., Lyne A. G., Johnston S., 2007, A&A, 462, 257
 Biggs J. D., 1992, ApJ, 394, 574
 Bruck Y. M., Ustimenko B. Y., 1979, A&A, 80, 170
 Davies J. G., Lyne A. G., Smith F. G., Izvekova V. A., Kuz'min A. D., Shitov Yu. P. 1984, MNRAS, 211, 57
 Deshpande A. A., Rankin J. M., 1999, ApJ, 524, 1008 (DR99)
 Deshpande A. A., Rankin J. M., 2001, MNRAS, 322, 438 (DR01)
 Gil J. A., Lyne A. G., Rankin J. M., Snakowski J. K., Stinebring D. R., 1992, A&A, 255, 181
 Hankins T. H., Rankin J. M. 2006, ApJS, submitted
 Harding A. K., Muslimov A. G., 1998, ApJ, 500, 862
 Herfindal J. L., Rankin J. M. 2007, MNRAS, in press (doi:10.1111/j.1365-2966.2007.12089.x)
 Janssen G. H., van Leeuwen A. G. J., 2004, A&A, 425, 255
 Lyne A. G., Ashworth M., 1983, MNRAS, 204, 519
 Lyne A. G., Manchester R. N., 1988, MNRAS, 234, 477
 Mitra D., Rankin J. M., 2002, ApJ, 577, 322 (MR02)
 Phillips J. A., Wolszczan A. 1989, ApJ, 344, L69

- Pilkington J. D. H., Hewish A., Bell S. J., Cole T. W., 1968, Nat, 218, 126
 Radhakrishnan V., Cooke D. J., 1969, Astrophys. Lett., 3, 225
 Rankin J. M., 1983, ApJ, 274, 333
 Rankin J. M., 1986, ApJ, 301, 901
 Rankin J. M., 1993a, ApJ, 405, 285 (R93a)
 Rankin J. M., 1993b, ApJS, 85, 145 (R93b)
 Redman S. R., Wright G. A. E., Rankin J. M., 2005, MNRAS, 375, 859 (RWR)
 Ritchings R. T., 1976, MNRAS, 176, 249
 Ruderman M. A., Sutherland P. G., 1975, ApJ, 196, 51
 Slee O. B., Mulhall P. S., 1970, Astrophys. Lett., 8, 5
 Srostlik Z., Rankin J. M., 2005, MNRAS, 362, 1121
 Taylor J. H., Jura M., Huguenin G. R., 1969, Nat, 223, 797
 van Leeuwen A. G. J., Kouwenhoven M. L. A., Ramachandran R., Rankin J. M., Stappers B. W., 2002, A&A, 387, 169
 van Leeuwen A. G. J., Kouwenhoven M. L. A., Stappers B. W., Ramachandran R., Rankin J. M., 2003, A&A, 399, 223
 Weltevrede P., Edwards R. T., Stappers B. W., 2006, A&A, 445, 243
 Weltevrede P., Stappers B. W., Edwards R. T., 2007, A&A, submitted
 Wright G. A. E., 2003, MNRAS, 344, 1041

APPENDIX A: CAROUSEL MODEL

A1 Underlying emission geometry

Specifications of the emission geometry of B0834+06 have been given by both Lyne & Manchester (1988) and Rankin (1993a,b; hereafter R93a,b), but both were based on average-polarization data which, as we have seen, are especially problematic for this pulsar, given the near parity of power in its OPMs. The latter model was computed using a PA sweep rate R of 8.5 deg^{-1} , which we have seen above is flatter than what is indicated by our observations. A better value is about twice this, $+17^\circ \pm 3^\circ \text{ deg}^{-1}$. Fortunately, this substantial uncertainty falls in a region of parameter space which does not make a large difference for our purposes, because the sightline traverse through the emission cone is in any case highly central and the profile width is nearly independent of wavelength: the R93b analysis used a profile width of 7.5 and the older R value, giving magnetic latitude α and sightline impact β of 30° and 3.4 , respectively; whereas our single-pulse R of $+17^\circ \text{ deg}^{-1}$ gives α and β values of 50° and 2.6 . In both cases, the emission-cone radius to the outer half-power point is 3.9 (as in MR02 as well). This analysis cannot, of course, determine the sign of β .

A2 The carousel circulation time

To understand how the nulling and subpulse modulation are closely related in pulsar B0834+06, we made every effort to determine the circulation time of its carousel. Overall, fluctuation spectra provide little indication regarding a low-frequency cycle in this star (e.g. Fig. 2), in part perhaps because null clustering tends to introduce ‘red’ noise. Careful study of shorter PSs with specific behaviours, however, did result in identifying some possible circulation features, but such features were unusual – and hardly of a clear and obvious significance. However, in certain short intervals the modulating beamlet configuration appears stable enough that a tentative analysis can be made.

We carried out various searches for the carousel circulation time \hat{P}_3 using the inverse-cartographic methods described in DR01. Here, various parameters including \hat{P}_3 are first used to construct a beamlet map; this map is used to compute an artificial PS, which is then correlated against the natural PS. After initially attempting searches with

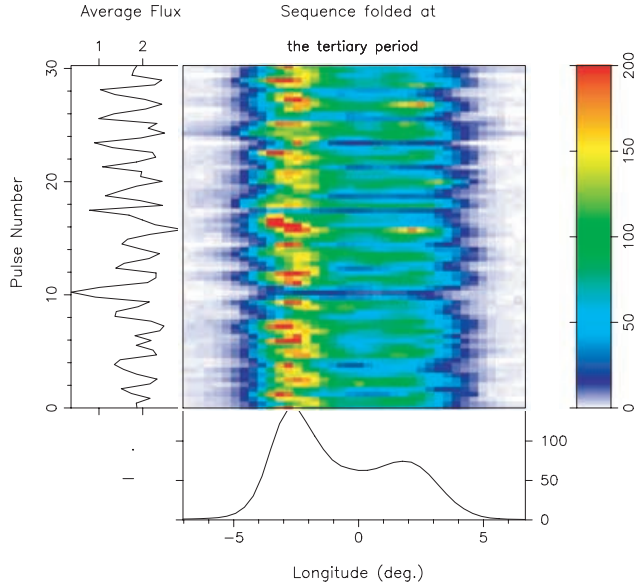


Figure A1. PSs folded at the putative circulation time \hat{P}_3 of $30.26P_1$, pulse # 3500–3700. This PS is one of the very most regular as seen earlier in Figs 3 (right-hand column), 4 (right-hand panel) and 5. The left-hand panels give the integrated power and the bottom ones the average profile.

a large range of interval lengths and \hat{P}_3 values, we then restricted them to 201-pulse segments and circulation times which represented various multiples of the best primary $2.161 \pm 0.011P_1 P_3$ or its alias. These searches were carried out using those sections (# 500–1400 and 3200–3789) of Fig. 6 that exhibited the most ordered behaviour. \hat{P}_3 values between about 11 and $43P_1$ were assessed. Overall, this analysis showed that circulation times which were multiples of $2.161P_1$ gave higher correlations than those of its feature alias. We also found that no \hat{P}_3 values smaller than $30P_1$ ($14P_3$) gave adequately large correlation values (60–70 per cent) together with sufficiently small modulation-phase differences (0.5 rad). Moreover, certain trial values of \hat{P}_3 longer than $30P_1$ did meet the above criteria, but not for all intervals.

We thus tentatively identify $30.26 (= 14 \times 2.1613)P_1$ as B0834+06’s probable circulation time \hat{P}_3 . A key question is then whether PSs folded at this interval exhibit the expected deep crenellation, produced jointly by the drift and the nulls, and indeed they appear to do so. Fig. A1 gives a set of profiles folded at the (tertiary) modulation period \hat{P}_3 corresponding to the highly regular PS seen previously in Figs 3 (right-hand column), 4 (right-hand panel) and 5. Here a clear pattern of 14 peaks is seen, many with roughly equal maxima, minima and spacing, just the pattern needed to produce the usual 0.461 -cycles/ P_1 modulation feature. We also carried out these folds with \hat{P}_3 values larger and smaller by up to 0.12; overall, $30.26 \pm 0.01P_1$ gave the largest modulation depths.

This putative \hat{P}_3 value of $30.26P_1$ then appears plausible, but it differs from that found by AD05, so some explanation is required. First, our analyses provide no clear confirmation of these authors’ conclusion that the drift is positive. We had expected that we would easily be able to confirm this conclusion by the same means: that is, a longitude–longitude correlation map with a $2P_1$ delay such as AD05’s fig. 5. Surprisingly however, our observations correlate in a more complicated manner. The reasons for this may well be

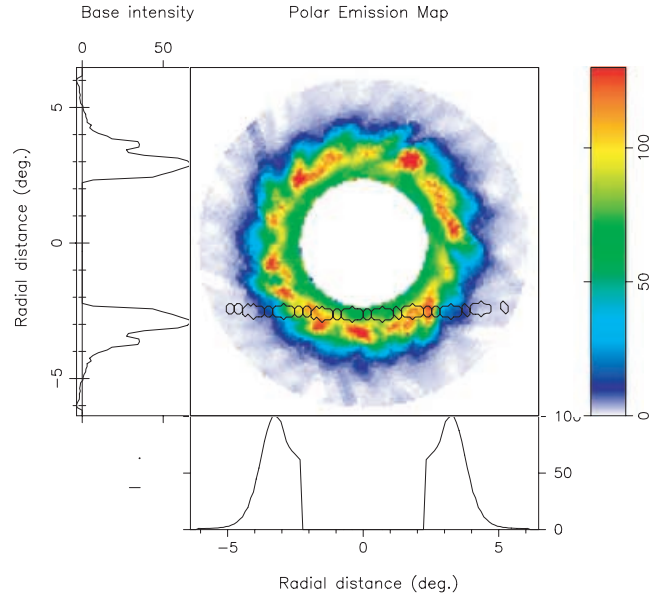


Figure A2. Subbeam carousel map (central panel) produced, using the cartographic mapping methods described in DR01, for pulse # 3500–3700 seen in Figs 3 (right-hand column), 4 (right-hand panel), 5 and 6 (right-hand panel). Here, the putative $30.26P_1$ \hat{P}_3 value has been used along with a negative drift and α , β values of 50° , $2:6$, respectively. The bottom panel gives the radial emission profile and the side panel the unmodulated base (which has not been subtracted from the central emission patterns). The sightline path is shown in contours for an (assumed) outer traverse.

very interesting⁴ but are beyond the scope of the current analysis. In any case, our analyses seem most compatible with a drift towards earlier longitudes (i.e. negative) – thus with a P_3 of 2.16 – $2.17P_1$. The aliasing issue is subtle for stars with P_3 values close to $2P_1$, and our analyses in no way fully settle the question. Secondly, our suggested circulation time is roughly twice that found by AD05, and this difference may be easier to understand. Several sections of our observations also show a $15P_1$ cycle as we have seen in Fig. 9, but this cycle seems to be a harmonic of \hat{P}_3 as both our inverse-cartographic modelling and analyses of particular intervals strongly suggest. Indeed, the greater prevalence of $15P_1$ features might argue that the true \hat{P}_3 has to be a subharmonic of this period (thus tending against certain longer intervals which also produce strong inverse-cartographic search results – for example, $41.065P_1$ or $19P_3$).

Another way of looking at these PSs is to construct cartographic beamlet maps using the methods described in DR01, and a polar carousel map corresponding to the folded PS in Fig. A1 is presented in Fig. A2 (representing the regular pulse # 3500–3700 sequence). Here, as in Fig. A1 we see evidence of a rough 14-beamlet emission pattern. Some of the beamlets are weaker, but much of the lower half of the carousel pattern is of a consistent spacing and brightness. It is then hardly surprising that this PS results in the narrow fluctuation-spectral feature of Fig. 4 (right-hand panel). Overall,

⁴ We suspect that this complex correlation can be traced to the properties of the polarization modes. Recall that in B0834+06 there is nearly equal power in the two modes across most of its profile – thus the nearly complete depolarization – and the modes appear to participate strongly in the modulation.

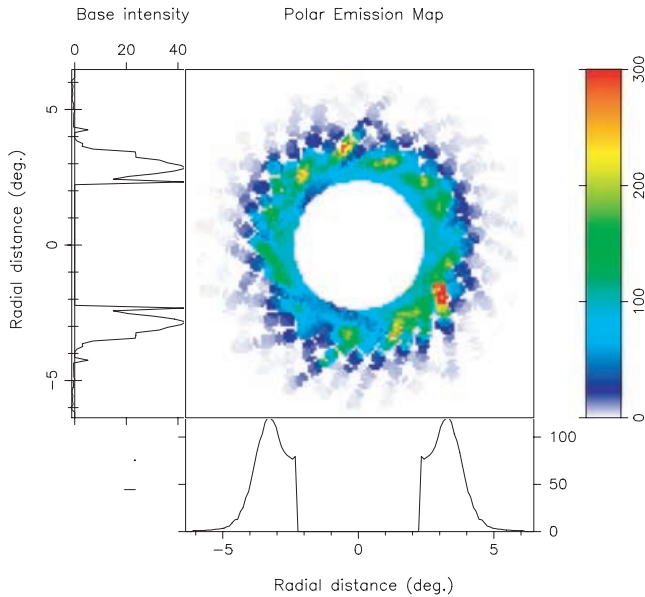


Figure A3. Carousel map as in Fig. A2 for a single circulation-time interval corresponding to the $30\text{-}P_1$ putative P_3 (pulse # 2521–2550). This short PS contains two apparent nulls, and the effects of both can be seen in the map as low intensity or missing parts of the pattern comprising successive sightline traverses. Note that these two tracks are partially erased by the traverses of other pulses occurring at different times. This map is one frame of a beamlet-carousel movie made as a means of viewing the star’s PS behaviour.

the star’s carousel configuration is not very stable as we have seen above in a variety of ways. A consequence is that much of the ‘fuzziness’ in the polar map of Fig. A2 is the result of averaging over a number of circulation times – averaging, that is, over beamlets that clearly vary considerably in both intensity and position in a circulation time.

In order to study the carousel configurations on the shortest possible time-scale, we have made polar maps of our observations using individual 30-pulse segments (‘frames’) corresponding to the putative circulation time and then joined them into ‘movies’. On this scale the effects of typically two or three ‘nulls’ can be seen clearly in virtually every frame. Not only does the ‘missing’ emission result in weak or absent contributions to the map, but one can see how particular traverses and carousel patterns set up conditions where empty sightline passes can occur. Of course, we cannot reproduce the ‘movie’ here,⁵ but we give a single frame as example in Fig. A3. Two apparent nulls occurred in this 30-pulse interval, and their effects can be seen clearly. The null tracks, of course, do not have a zero intensity because adjacent pulses, in crossing them, contribute some intensity. And here the width of the sightline traverse is overemphasized for clarity, but this also contributes to filling in the null track.

⁵ The full movie can be downloaded from <http://www.uvm.edu/~jmrankin> under ‘Research’ and ‘Images and Movies’.

This paper has been typeset from a $\text{\TeX}/\text{\LaTeX}$ file prepared by the author.